Wave activity above the ionosphere of Titan: Predictions for the Cassini mission

Zoltán Dóbé[1] and Károly Szegő

Központi Fizikai Kutató Intézet Research Institute for Particle and Nuclear Physics, Budapest, Hungary

Received 19 April 2004; revised 4 August 2004; accepted 14 October 2004; published 29 March 2005.

[1] In this paper we present a study of the beam-driven wave generation mechanisms in linear approximation which are viable in the flowside plasma mantle of Saturn's moon, Titan. The flowside plasma mantle is defined, by analogy with the dayside plasma mantle of the planet Venus and Mars, as being the interaction region between the "cold" ionospheric plasma and "hot" streaming plasma of magnetospheric or solar wind origin, with both types of plasma being present in comparable densities. Since no in situ plasma and field measurements are currently available in Titan's flowside mantle, we performed our model calculations in a broad plasma parameter space encompassing the plasma characteristics determined by Voyager 1 in Titan's wake. Two types of beam instability modes were found to be dominant: a fluid-like (nonresonant) modified two-stream instability (MTSI) and the kinetic (beam resonant) ion-ion acoustic instability (IIAI). The two instability modes are characterized by distinct frequency ranges (an order or below the lower hybrid frequency for the MTSI and a few times the lower hybrid frequency for the IIAI) and are found to be dominant in well-separated spatial regions determined by the presence/absence of cold ionospheric electrons. Giving a global rather than a specific description of the instability types expected to be the most important growing modes within Titan's flowside mantle, we intend to make predictions concerning the wave characteristics of the dominant wave modes measurable by the plasma wave instrument on board the Cassini spacecraft.

Citation: Dóbé, Z., and K. Szegő (2005), Wave activity above the ionosphere of Titan: Predictions for the Cassini mission, *J. Geophys. Res.*, *110*, A03224, doi:10.1029/2004JA010548.

1. Introduction

[2] The exploration of Titan, the largest moon of Saturn, is one of the main objectives of the Cassini mission. Forty-four flybys are planned at various encounter distances from this moon, and close observations will be made of the plasma features at Titan. Titan is the largest moon of Saturn, orbiting it from a distance of 1,220,000 km ($\sim$20.2 R_S, where R_S is the radius of Saturn) in $\sim$15.95 days (sidereal period); its radius R_T is 2575 km, and it possesses a dense atmosphere [*Hunten et al.*, 1984], having an exobase of $\sim$1430 km from the surface. Voyager 1 flew across Titan's plasma wake on 12 November 1980 when the moon was inside Saturn's magnetosphere. Cassini will explore Saturn between 2004 and 2006, i.e., $\sim$2.3 solar cycles later during low–solar activity conditions.

[3] The characteristic properties of the interaction of Titan with its plasma environment are determined by two major factors.

[4] 1. Because of Titan's nonexistent or very weak intrinsic magnetic field the surrounding plasma flow has direct access to the upper atmosphere and exosphere (similar to the case of Venus, Mars, or comets). During the Voyager 1 encounter this flow was deflected by $\sim$20° relative to the corotation direction.

[5] 2. Titan's orbit passes through different plasma regions around Saturn: It may cross the magnetosheath, the corotation region, and the plasma associated with Saturn's tail, and when the solar wind pressure is high, a portion of the orbit is in the unperturbed solar wind.

[6] According to the Voyager 1's measurements, when Titan was located within the magnetosphere of Saturn, the plasma in the vicinity of Titan was composed of H^+ and N^+ ions, with densities of 0.1 and 0.2 cm^{-3} and temperatures of about 210 eV and 2.9 keV, respectively. The temperature of the magnetospheric electrons in the neighborhood of Titan is of the order of 200 eV. The measured mean plasma flow speed outside the wake of Titan is $\sim$120 km s^{-1}, and the magnetic field is of the order of 5 nT (*Hartle et al.* [1982], *Ness et al.* [1982], and for a review, see also *Neubauer et al.* [1984] and *Neubauer* [1992]). On the basis of these parameters the flow is subsonic (sonic Mach number $M_S \sim 0.6$) and trans-Alfvénic (Alfvénic Mach number $M_A \sim 1.9$). The analysis of the Voyager 1 data gained in the wake of

[1] Also at General Electric Consumer and Industrial Products, Budapest, Hungary.

0148-0227/05/2004JA010548$09.00

Titan showed a complex interaction between the upper atmosphere of Titan and the magnetosphere of Saturn, where finite gyroradius effects are essential. The presence of pickup ions near Titan was detected by the plasma science instrument on board Voyager 1 and was also supported by the increased wave activity level observed by the plasma wave system instrument during the inbound approach. More recently, *Sittler et al.* [2004] and E. C. Sittler et al. (Titan interaction with Saturn's magnetosphere: Voyager 1 results revisited, submitted to *Journal of Geophysical Research*, 2004) revisited the original plasma data analysis of *Hartle et al.* [1982] and showed that in the outer pickup region, ion pickup of H^+ and H_2^+ dominates, while the plasma flow experienced major mass-loading effects when it reached the exospheric population dominated by heavy neutral species. It was also shown that finite gyroradius effects resulted in an asymmetric removal of the ambient plasma from Titan's exospheric region.

[7] When Titan reaches the magnetosheath or the unperturbed solar wind, the streaming plasma consists mainly of protons. So far, no in situ measurements are available characterizing the plasma properties of the magnetosheath or unperturbed solar wind near Titan. According to the model calculations of *Wolf and Neubauer* [1982], for an unperturbed solar density of 0.1 cm^{-3} and bulk velocity of 400–500 km s^{-1} the stagnation point of shocked solar wind is at a distance of $\sim$17 R_S from Saturn's center, so Titan will be located in the magnetosheath for an appreciable fraction of time [*Acuna and Ness*, 1980]. In this case the shocked solar wind proton density varies around a few times 0.1 cm^{-3}, and velocity is 100–300 km s^{-1}, while the plasma temperature (sum of the electron and proton temperature) is about $7-8 \times 10^7$ K. The interplanetary magnetic field within the magnetosheath is about the order of 1–2 nT, resulting in a plasma beta of the order of >1. (We note, however, that Cassini measured much lower sheath temperature at Jupiter.)

[8] The ionosphere of Titan is formed by three different ionization processes: (1) photoionization by solar extreme ultraviolet radiation, (2) electron impact ionization, and (3) charge transfer of flowing plasma with neutrals. For planets the first source dominates on the dayside, although the second source (electron impact ionization) can make a significant contribution if the electron energies are elevated [*Zhang et al.*, 1993]. In the mantle regions of Venus and Mars the charge transfer interaction of solar wind protons with neutral oxygen, in which the protons are removed from the flow and are replaced by heavy ions initially at rest, makes a contribution to mass loading. For satellites in the inner magnetospheres of outer planets (e.g., Io and Europa at Jupiter), electron impact ionization associated with energetic magnetospheric electrons is more important than photoionization. On the nightside of Venus and Mars, other ionization processes form the nightside ionosphere. Around Titan, when the moon is inside the corotation region, the position of the Sun relative to corotating plasma flow direction varies and significantly increases the complexity of the plasma interaction. The relative importance of the ionization processes in the case of Titan was discussed by *Nagy and Cravens* [1998]; they concluded, in agreement with *Keller et al.* [1992], that the main source is photoionization, followed by photoelectron impact and finally magnetospheric electron sources (impact ionization due to the corotating flow can be $\sim$20% of solar EUV). Evidently, the structure of Titan's ionosphere inside magnetosphere depends on the relative angle of the directions of the particular ionization process.

[9] At Titan, kinetic effects associated with the impinging plasma may further complicate the ionosphere structure. In a global hybrid simulation reported by *Brecht et al.* [2000] the scale of the interaction region was dominated by the heavy ion gyroradii of the ambient and pickup ions rather than by the size of Titan and was found to depend on the mass loading of the magnetospheric flow encountering Titan. *Kopp and Ip* [2001] also pointed out that since the gyroradius of N^+ ions in the impinging flow can be much bigger than R_T, such ions might be recaptured on the other side, contributing to ionospheric heating. Though *Hartle et al.* [1982] attempted a kinetic description of the plasma environment of Titan, current models [*Cravens et al.*, 1998; *Ledvina and Cravens*, 1998; *Kabin et al.*, 2000] assume that a MHD description of the interaction of the impinging plasma with Titan's ionosphere is an acceptable approximation.

[10] Several hydrodynamic and MHD models were developed in recent years describing the composition and thermal structure of Titan's ionosphere [see, e.g., *Keller et al.*, 1992; *Roboz and Nagy*, 1994; *Cravens et al.*, 1998]. The main ionization and heat sources incorporated in these ionospheric models are solar EUV radiation and impact ionization of energetic electrons of magnetospheric or solar wind origin. The resulting dominant ion species within the topside ionosphere were given the generic name of mass 28 amu ($C_2H_5^+$, H_2CN^+, and N_2^+), and the ion temperatures turned out to be extremely cold, of the order of $T_I \sim 0.035$ eV. The temperature of the thermal component of the ionospheric electrons is in the range of 2–3 times the cold ion temperature.

[11] The objective of this and a forthcoming paper is to predict possible wave excitation modes and ion distributions observable during Cassini flybys, characteristic of regions around Titan, where streaming plasma is directly impinging Titan's ionosphere. We call this plasma region here the "flowside" mantle in analogy to the dayside mantle region of Venus and Mars [*Spenner et al.*, 1980; *Lundin et al.*, 1990; *Nagy et al.*, 1990, and references therein] because in this region around Titan both the ionospheric plasma and the plasma of the impinging flow are present in comparable number densities. The ionospheric plasma can arise within the plasma mantle from newly photoionized, impact-ionized, or charge-exchanged neutrals originating from the upper atmosphere of Titan or may escape from the ionosphere into the hot magnetospheric plasma or solar wind.

[12] Theoretical studies support the idea that significant collisionless momentum and energy exchange are taking place in this transition region because of wave-particle interaction, resulting in a highly turbulent layer, where even the bulk properties of the plasma would significantly change because of this so-called "anomalous viscosity" [*Sagdeev et al.*, 1990]. Two types of instability modes were proposed as explanations of the observed wave

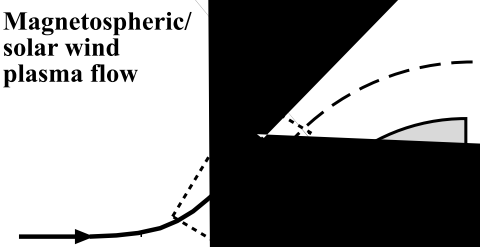

analyzer on board Cassini on the saturated wave electric field energy and energy distribution function of the superthermal particles accelerated by nonlinear wave-particle interactions.

2. Linear Dispersion Relation Analyses of Beam Instabilities

[18] We also used the unmagnetized ion approximation which is valid for waves with characteristic timescales much larger than the gyroperiod of the ion cyclotron motion and for wavelengths much smaller than the ion gyroradius. It is also assumed that electron cyclotron damping is unimportant, i.e., $(\omega_e/\sqrt{2}k_{\|}\ V_{Te})^2 \gg 1$. The

$_0$ is $k_{\|}$. Without losing generality we can

Following *Wu et al.* [1983], the dispersion relation can be written as follows:

$$1 + \sum_{p,N+,I} \frac{1}{k^2\lambda_i^2}[1 + w_i Z(w_i)] + \sum_{c,h} \frac{1}{k^2\lambda_e^2}[1 + w_e Z(w_e) K_0(\mu)] + \mathrm{EM} = 0, \tag{1a}$$

where

$$\mathrm{EM} \equiv \sum_{c,h} \frac{\omega_{pe}^4}{k^4 c^2 v_{Te}^2} \cdot \frac{\left\{\frac{4\omega_{pe}^2}{k^2c^2}\Phi_2\Phi_3\Phi_4 + \Phi_3^2\left[1 + \frac{2\omega_{pe}^2}{k^2c^2}\Phi_1\right] + \Phi_2^2\left[1 + \frac{2\omega_{pe}^2}{k^2c^2}\Phi_5\right]\right\}}{\left[1 + \frac{2\omega_{pe}^2}{k^2c^2}\Phi_5\right]\left[1 + \frac{2\omega_{pe}^2}{k^2c^2}\Phi_1\right] - \left[\frac{2\omega_{pe}^2}{k^2c^2}\right]^2 \Phi_4^2}, \tag{1b}$$

where

$$\Phi_1 \equiv -wZ(w)\mu e^{-\mu}(I_0 - I_1),$$
$$\Phi_2 \equiv -\left(\sqrt{2}/2\right)wZ(w)\sqrt{\mu}e^{-\mu}(I_0 - I_1),$$
$$\Phi_3 \equiv -w[1 + wZ(w)]e^{-\mu}I_0,$$
$$\Phi_4 \equiv \left(\sqrt{2}/2\right)[1 + wZ(w)]\sqrt{\mu}e^{-\mu}(I_0 - I_1),$$
$$\Phi_5 \equiv -w^2[1 + wZ(w)]e^{-\mu}I_0.$$

Here $Z(\xi)$ is the plasma dispersion function $Z(\xi) = i\sqrt{\pi}\exp(-\xi^2)[1 + \mathrm{erf}(i\xi)]$, where erf is the error function, $K_0(\mu) = I_0(\mu)e^{-\mu}$, I_n is the Bessel function of nth order, and $\mu \equiv k_\perp^2\rho_e^2/2$, where $k_\perp$ is a vector component of $\mathbf{k}$ perpendicular to $\mathbf{B}_0$. The resonance term w corresponds to different charged particle populations. In the case of magnetized electrons, $w_e = (\omega - \mathbf{k}\mathbf{U}_e)/\sqrt{2}k_\parallel V_{Te}$; similarly, in the case of unmagnetized ions, $w_i = (\omega - \mathbf{k}\mathbf{U}_i)/\sqrt{2}kV_{Ti}$, where i represents protons, N^+ ions, and ionospheric ions.

[19] Here we have presumed that the reference frame is linked to Titan (the ionospheric ion drift velocity is zero). The bulk velocity of the electrons is determined by the current neutrality assumption used throughout this study. This means that the drift velocity of the electron population is determined in such way that $\Sigma_j q_j n_j \mathbf{U}_{0j} = 0$, where q_j, n_j, and $\mathbf{U}_{0j}$ are the electrical charge, number density, and drift velocity of the jth type of charged particle. Current neutrality is a consequence of the absence of the magnetic shear and is also required by the one-dimensional hybrid particle-in-cell simulation describing the wave evolution within the plasma mantle used in a forthcoming paper. For the sake of consistency we introduce current neutrality here as well. It can be proven that releasing this condition in the analytic dispersion relation does not alter the physical nature and evolution of the instability modes discussed, at least in their linear stage.

3. Parameter Dependence of the Wave Excitation Processes in the Flowside Mantle of Titan

[20] In this study we analyze how the solution $\omega + i\gamma$ of the general dispersion relation (1) depends on independent, dimensionless plasma parameters such as ion beam drift velocity normalized to the proton thermal velocity, ion beam number density normalized to the total electron density, beam ion and electron temperature normalized to the ionospheric ion temperature, ionospheric ion mass normalized to the proton mass, and electron plasma beta ($\beta_e = 8\pi k_B n_e T_e/B_0^2$).

[21] By analogy with the Venus and Mars dayside mantle, two instability types generated by the relative drift between the different plasma components existing within the flowside mantle of Titan were considered: "lower hybrid–type" instability modes with characteristic frequencies in the vicinity of the local proton lower hybrid frequencies and "ion acoustic–type" instability modes ranged at somewhat higher frequencies of the order of the local ionospheric ion plasma frequency. In the case of the lower hybrid–type instabilities the presence of magnetized electrons is needed. The instability mode driven by the relative drift between two unmagnetized ion components gives rise to the so-called lower hybrid drift instability (LHDI) waves which typically propagate in a very narrow range of angles close to directions perpendicular to the external magnetic field. More obliquely propagating waves are generated by the so-called modified two-stream instability (MTSI) scenario driven by the relative cross-field drift of unmagnetized ions and magnetized electrons. (For a detailed discussion of the properties of these modes, see, for example, *Wu et al.* [1983], *Bingham et al.* [1991], and *Shapiro et al.* [1995].) In the case of higher electron temperatures ($T_e \gg T_I$) the wave dispersion properties become similar to those of ion acoustic waves. Using the nomenclature of *Gary and Omidi* [1987], two types of instability branches can be distinguished: electron-ion and ion-ion acoustic instabilities (IIAI), depending on whether the relative drift driving the instability is between electrons and ions or ions and ions. It is important to note that the ion acoustic–type instability modes are insensitive to the presence of the background magnetic field since the dominant wavelengths are of the order of the Debye length and are much shorter than the electron gyroradius, i.e., $k_\perp^2\rho_e^2 \gg 1$.

[22] Because of their fluid nature the LHDI waves are strongly quenched at beam ion temperature ranges characteristic to the proton and nitrogen ions measured by Voyager 1 within Saturn's magnetosphere, so we do not consider this instability branch for Titan's flowside mantle in this paper. Analyses of the dispersion relation (1) show that two different, predominantly electrostatic MTSI modes may exist. One is of a kinetic-type branch having frequencies several times the lower hybrid frequency and being the result of the resonant interaction between solar wind protons and cold, magnetized ionospheric electrons, as proposed by *Shapiro et al.* [1995] for Venus. Because of its kinetic nature this branch develops much slower than the second, fluid-type MTSI mode for beam ion temperatures characteristic to flowside Titan mantle. These waves have characteristic frequencies below the lower hybrid frequency and are generated by nonresonant interaction between the cold, ionospheric ions, i.e., $w_I = \omega/\sqrt{2}kV_{TI} \gg 1$, and the magnetized electron beam, also originating from the ionosphere, i.e., $w_e = (\omega - \mathbf{k}\mathbf{u}_e)/\sqrt{2}k_\parallel V_{Te} \gg 1$, and created by fast $\mathbf{E} \times$

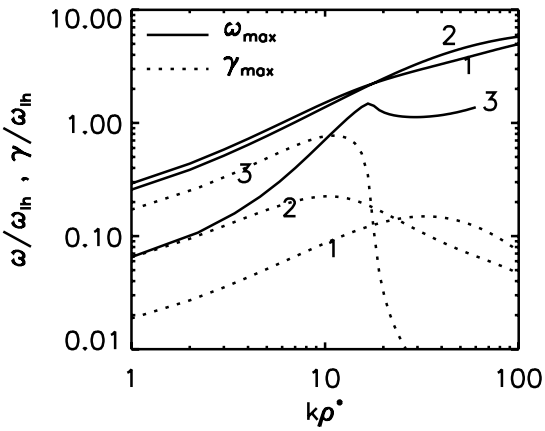

Figure 2. Variation of normalized frequency, ω_m/ω_{LH} (solid line), and growth rate, γ_m/ω_{LH} (dotted line), in function of normalized wave number, $k_m\rho^*$, at three different ratios of cold to total electron number densities, n_{ec}/n_e: 0.01% (ion-ion acoustic instability (IIAI) mode, lines 1), 0.1% (lines 2), and 2% (modified two-stream instability (MTSI) mode, lines 3). These results correspond to average beam plasma parameters close to the ones measured by Voyager 1 at Titan [*Hartle et al.*, 1982]: U_b = 120 km s^{-1}, n_p = 0.1 cm^{-3}, n_{N+} = 0.2 cm^{-3}, T_p = 210 eV, T_{N+} = 2.9 keV, and $T_{e,hot}$ = 200 eV. External magnetic field is B_0 = 5 nT [*Ness et al.*, 1982]. Ionospheric ion and electron temperatures were calculated by *Roboz and Nagy* [1994]: T_I = 0.035 eV and $T_{e,cold} \sim 2\ T_I$. The mass of the dominant ionospheric ion species was taken to be m_I = 28 amu. Specific angles of wave propagation used in these calculations correspond to the fastest-growing mode: θ = 83.5° and α = 0°, where θ and α are wave propagation angles relative to the external magnetic field and bulk velocity vector, respectively.

B pickup. Electron pickup takes place over a few electron gyroperiods, a time interval much shorter than the lower hybrid period. According to *Dóbé et al.* [1999], although the cold electron beam has little kinetic energy of its own, the wave-particle resonance is sustained for a longer time because of electron pickup under the combined action of the magnetic and convective electric fields of the solar wind. This makes possible a substantial transfer of free energy from streaming plasma flow to the waves already at the initial linear wave growth stage.

[23] The scenario of ion acoustic–type wave generation is quite different since in this case the instability mode is of resonant type, i.e., $w_{e,I} = (\omega - ku_{e,I})/\sqrt{2}kV_{Te,I} < 1$, and is driven by inverse Landau damping. Accordingly, the growth rate very much depends on the slope of the velocity distribution function of the charged beam particles (electrons and ions) moving within the resonance velocity range enclosing the wave phase velocity. This feature will be further discussed in section 3.2.

[24] Another important feature of the ion acoustic mode is its sensitivity to the electron temperature or, more specifically, to the presence of the cold electron component originating from the ionosphere. In Figure 2 the wave frequency and growth rate normalized to ω_{LH} are shown as a function of wave number normalized to $\rho^* = V_{Tp}/\omega_{LH} = \sqrt{(T_p/T_e)}\rho_e$ (scale length comparable to electron gyroradius calculated with proton temperature) for three different values of cold electron number densities: $n_{ec}/n_e = 10^{-4}$ (line 1), 10^{-3} (line 2), and 2×10^{-2} (line 3). The results demonstrate how the dominant ion-ion acoustic branch is stabilized because of Landau damping by the presence of a cold electron population at relative number densities as low as ~1%. It can be seen that even at these cold electron density ratios the dominant instability is the cold electron beam-driven MTSI mode and the frequency corresponding to maximum growth rate is below ω_{LH}. By gradually decreasing the density of cold electrons from $n_{ec}/n_e = 2 \times 10^{-2}$ to 10^{-4} the IIAI waves become dominant with typical real frequencies in the range of a few times ω_{LH}, close to the ionospheric ion plasma frequency. Correspondingly, the two types of instability modes in the simultaneous presence of substantial cold and hot electron densities cannot exist together. This behavior of the ion acoustic branch was already discussed by *Szegő et al.* [2000] for conditions relevant to the plasma mantles of Venus and Mars. Here we just want to further emphasize the importance of this behavior, which enables us to conclude that it is sufficient to describe the electron population by a single-temperature Maxwellian distribution function, corresponding to either cold electrons (of ionospheric origin) with typical temperature of the order of a fraction of eV or hot electrons (of magnetospheric or solar wind origin) with characteristic temperatures of the order of a hundred eV. In sections 3.1 and 3.2 we separately investigated the model parameter dependence of the two dominant instability modes.

3.1. Modified Two-Stream Instability

[25] Figure 3 shows the solution of the dispersion relation (1) corresponding to the MTSI mode for different ion beam velocities ($u \equiv U_b/V_{Tp}$ = 0.5, 1, 2, and 3) as a function of wave propagation angles relative to the external magnetic field, $\theta = \arccos(k_{||}/k)$. For fixed θ values we have calculated the wave frequencies, ω_m (Figure 3a), and wave numbers, k_m (Figure 3c), corresponding to growth rates, γ_m, maximized over the wave numbers (Figure 3b). The frequencies and growth rates are normalized to the lower hybrid frequency, $\omega_{LH} = (\omega_{cp}\omega_{ce})^{1/2}$, while the corresponding wave numbers to electron gyroradius are calculated with proton temperature, $\rho^* = (T_p/T_e)^{1/2}\rho_e$. Here and in the following results the direction of propagation of the MTSI waves is constrained to lie within the plane defined by the directions of ambient magnetic field and the relative plasma drift velocity vector. With the use of sample calculations one can demonstrate that the maximum growth rate for these types of waves does correspond to this case.

[26] An analytic approximation of the MTSI-type solution of the general dispersion is also shown for comparison (thick solid line labeled "An.Sol." in Figure 3) for the case of u = 1. In the magnetized, cold fluid electron approximation, corresponding to the case when the electron resonance term $w_e = |(\omega - \mathbf{kU}_e)/\sqrt{2}k_{||}V_{Te}| \gg 1$, the electron plasma function can be approximated by the expression $Z(w_e) \cong -1/w_e$. The most unstable mode corresponds to the case when the Doppler-shifted wave frequency ($\omega - \mathbf{kU}_e$)

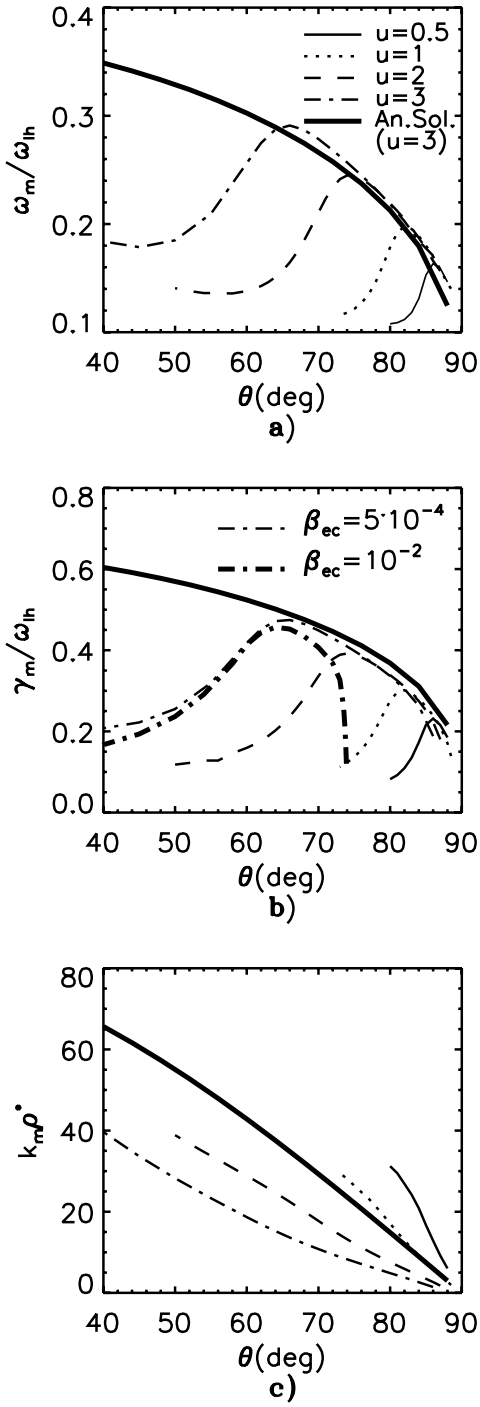

Figure 3. Beam velocity dependence of (a) wave frequency, ω_m/ω_{LH}, (b) growth rate, γ_m/ω_{LH}, and (c) wave number, $k_m\rho^*$, corresponding to the fastest growing MTSI modes. The beam velocities are $u \equiv U_b/V_{Tp} = 0.5$ (solid line), 1 (dotted line), 2 (dashed line), and 3 (dot-dashed line). All the general solutions of the dispersion equation (1) represented by thin lines correspond to electron plasma beta, $\beta_e = 5 \times 10^{-4}$, except the thick dot-dashed line in Figure 3b which represents the MTSI growth rate corresponding to $\beta_e = 10^{-2}$. Analytical approximation of the solution of dispersion relation in the case of $u = 1$ (corresponding to cold, magnetized fluid electrons) is represented by the thick solid line. Other relevant plasma parameters are fixed and identical to the ones used in Figure 2.

coincides with the frequency of the plasma eigenmode, which in our case is the whistler mode. (This is similar to the Bunemann instability in an unmagnetized plasma, when the plasma eigenmode coincided with the Langmuir frequency.) The fluid-type resonance condition can be written as

$$\mathbf{k}\mathbf{U}_e \approx \omega_{ce} k_\parallel k c^2 / \left(k^2 c^2 + \omega_{pe}^2\right), \tag{2}$$

determining the wavelength corresponding to maximum growth rate. We also can easily find an approximate solution corresponding to the resonance condition using the fluid electron approximation

$$\omega_m + i\gamma_m \approx \left(\frac{1}{2}\right)^{4/3} \left(\frac{n_i}{n_e}\frac{m_e}{m_I}\right)^{1/3} \left(\frac{k^2c^2 + \omega_{pe}^2}{k_\parallel^2 c^2}\right)^{1/3} \left(1 + i\sqrt{3}\right)\mathbf{k}\cdot\mathbf{U}_e, \tag{3}$$

where index m indicates the fastest growing mode. The effect of the beam protons and nitrogen ions on the linear evolution of the instability can be neglected because of their large drift velocity compared to the phase velocity of the MTSI waves.

[27] In this fluid electron limit, no electron Landau damping may occur, and the MTSI waves can propagate along arbitrary angles relative to the magnetic field. Both frequencies and growth rates are monotonically increasing with decreasing propagation angles independently of the beam drift velocity. As shown in Figure 3, the agreement between the analytically approximated and numerical solution breaks down when a significant part of the cold electron component becomes "more resonant" with the magnetized electron beam; that is, w_e becomes of the order of unity. In this regime the MTSI waves propagating on decreasing angles relative to the magnetic field lines are gradually Landau damped by cold electrons, and the fluid electron approximation loses its validity. Numerical results show that both the frequency and growth rate corresponding to different beam velocities show maxima at magnetized electron resonance term values, $|w_e|$, between 4 and 5. The maximum growth rates and the corresponding wave frequencies increase with increasing beam velocities. It can also be seen from Figure 3 that with increasing beam drift velocity the direction of propagation of the dominant modes becomes less perpendicular and the width of unstable propagation angle range increases. For a given beam drift velocity the wave numbers monotonically decrease with increasing propagation angles; however, the wave numbers corresponding to growth rates maximized over both wave numbers and propagation angles hardly change their values of $\sim 13/\rho^*$ with the beam velocity.

[28] It can be shown that the excited MTSI waves are predominantly electrostatic, i.e., $(\omega_{pe}/kc)^2 \ll 1$, for the cold electron plasma beta limit. For example, $\beta_e = 8\pi k_B n_e T_e / B_0^2 \sim 5 \times 10^{-4}$, calculated for the plasma parameters given in Figure 2. Using this electrostatic limit, we can further reduce the analytical expression (3) of the MTSI-type solution of the general dispersion relation (1) to $\omega_m + i\gamma_m \sim (1/2)^{4/3}(n_I/n_e)^{1/3}(m_p/m_I)^{1/3}\kappa^{1/3}(1 + i\sqrt{3})\omega_{LH}$ by

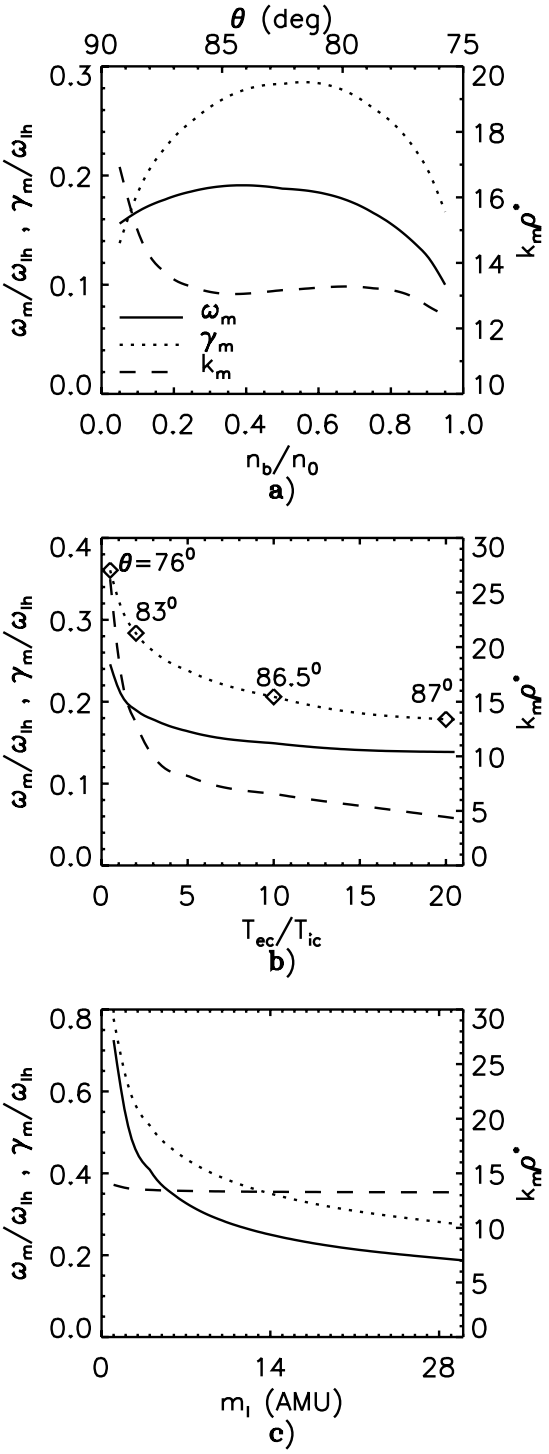

Figure 4. Dependence of the MTSI-type solution of the dispersion relation (1) on (a) beam density, n_b/n_e, (b) cold electron temperature, T_{ec}/T_I, and (c) ionospheric ion mass, m_I/m_p. The wave frequency, ω_m/ω_{LH} (solid line), growth rate, γ_m/ω_{LH} (dotted line), and wave number, $k_m\rho^*$ (dashed line), correspond to the fastest growing modes determined by maximizing growth rate over wave numbers and propagation angles (θ) relative to the magnetic field. Other plasma parameters are fixed and identical to the ones used in Figure 2.

assuming wave propagation parallel to the beam drift velocity, $\mathbf{kU}_e = kU_e$. Here we introduced the dimensionless variable $\kappa = (k_\parallel/k)\sqrt{(m_p/m_e)}$, measuring the angle of wave propagation relative to the external magnetic field, $\theta = \arccos[\kappa\sqrt{(m_e/m_p)}]$.

[29] However, finite beta effects may play an important role at higher beta values in the case of the MTSI mode. In order to demonstrate this effect, in Figure 3b we present (thick dot-dashed line) the solution of the dispersion relation (1) corresponding to the $u = 3$ case, using a somewhat higher electron plasma beta, $\beta_e = 10^{-2}$. (All other plasma parameters were kept unchanged.) It can be seen that for wave propagation directions close to perpendicular the MTSI mode was quenched or significantly reduced. This behavior can be analytically expressed by using the fluid electron approximation again. Accordingly, it can easily be shown that the instability can be stabilized by electromagnetic effects if $U_e/V_A^* \geq (1/2)\kappa$, where V_A^* is the Alfvèn velocity calculated with electron density and proton mass, $V_A^* = B_0/(4\pi n_e m_p)^{1/2}$. (A similar conclusion was derived previously by *McBride and Ott* [1972] for the electromagnetic effects on the MTSI on the basis of fluid description.) For a given beam velocity and electron plasma beta this relation can be translated to the condition for unstable wave propagation direction: $\kappa = (m_p/m_e)^{1/2}\cos\theta \geq (n_b/n_e)[2(T_P/T_e)\beta_e]^{1/2}u$.

[30] One can also easily demonstrate the consistency of the unmagnetized ion condition with the solution of the dispersion relation. By using the electrostatic form of the analytical approximation of the frequency and growth rate of the dominant MTSI waves we can approximate the ratio of the characteristic timescale of the fastest growing mode to the ion gyroperiod as $t_{MTSI}/T_{ci} \approx (1/2\pi)(n_e/n_I)^{1/3}(m_e/m_p)^{1/2}(m_I/m_p)^{1/3}(m_p/m_i)\kappa^{-1/3}$, resulting in values of the order of or less than 10^{-2} for considerable ionospheric ion densities, n_I ($n_I/n_e \sim 0.1$–0.9), and for all ion types (where i may represent protons, nitrogen ions, or ionospheric ions). Moreover, the dominant MTSI wavelength is compared to the gyroradius of the different ion species as $k_m\rho_i \approx \kappa(m_p/m_e)^{1/2}(m_i/m_p)^{1/2}(T_i/T_p)^{1/2}(n_e/n_b)u^{-1}$, where we make use of the resonance condition (2). At beam velocity comparable to proton thermal velocity, $u = U_b/V_{Tp} \sim 1$, and wave propagation direction, κ, corresponding to the fastest growing mode, it can be readily seen that $k_m\rho_{ci}$ is of the order of or greater than 10, where $\rho_i = v_{Ti}/\omega_{ci}$. Accordingly, we can conclude that the ion gyromotion does not significantly alter the evolution of the MTSI mode at least during the linear growth phase.

[31] Figure 4 shows the parameter dependence of the dominant MTSI mode on the beam density normalized to the electron density, n_b/n_e (Figure 4a); cold electron temperature normalized to the ionospheric ion temperature, T_{ec}/T_I (Figure 4b); and the ionospheric ion mass normalized to the proton mass, m_I/m_p (Figure 4c). During the calculations the rest of the parameters were kept at fixed values corresponding to the average plasma conditions observed by Voyager 1 spacecraft near Titan [*Hartle et al.*, 1982] and also determined by the ionospheric model calculations [*Roboz and Nagy*, 1994] used in Figure 2.

[32] Figure 4a illustrates the normalized characteristics frequency, ω_m (solid line), and wave number, k_m (dashed

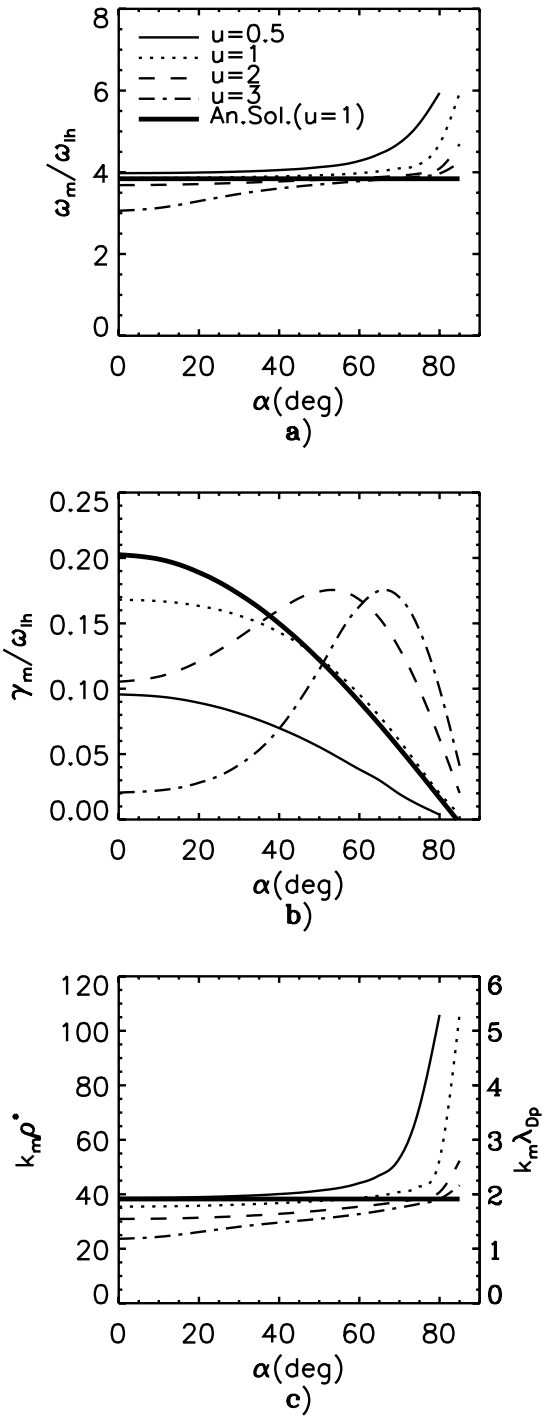

Figure 5. Beam velocity dependence of (a) wave frequency, ω_m/ω_{LH}, (b) growth rate, γ_m/ω_{LH}, and (c) wave number, $k_m\rho^*$, corresponding to the fastest growing IIAI modes. The beam velocities are $u \equiv U_b/V_{Tp} = 0.5$ (dotted line), 1 (solid line), 2 (dashed line), and 3 (dot-dashed line). The analytically approximated solution of the dispersion relation in the case of $u = 1$ (corresponding to hot, unmagnetized, kinetic electrons) is represented by the thick solid line. Other relevant plasma parameters are fixed and identical to the ones used in Figure 2.

line), corresponding to growth rate, γ_m (dotted line), maximized over wave numbers and propagation angles of the MTSI wave modes in function of the normalized beam density. Both the wave frequency and growth rate show maxima at slightly different corresponding beam densities and propagation angles relative to the magnetic field. The largest ω_m occurs at $n_b/n_e = 0.55$ and $\theta_m \sim 82°$, and the maximum of γ_m is at $n_b/n_e = 0.4$ and $\theta_m \sim 84°$. The dominant wave modes propagate at approximately linearly decreasing angles varying from $\theta_m = 88°$ to 77° while beam densities increase from 0.1 to 0.9.

[33] In Figure 4b we plot the wave characteristics of the fastest growing MTSI mode in function of the normalized ionospheric electron temperature. As we can readily see, the wave frequencies, growth rates, and wave numbers are monotonically decreasing, while the corresponding propagation angles, θ, are monotonically increasing with increasing ionospheric electron temperatures. This behavior is a consequence of the fact that an increase in the cold electron temperature, while keeping all other parameters constant, reduces the electron resonance term, $|w_{e,\mathrm{cold}}| \sim (\mathbf{k}/k)\cdot\mathbf{U}_e/\sqrt{(2\cos\theta V_{Te})}$ and increases the propagation angle of the dominant modes to values where the electron Landau damping becomes important. In other words, by increasing the ionospheric electron temperature the propagation angle corresponding to the maximum growth rate is becoming more perpendicular to the magnetic field lines, while the range of the unstable wave propagation angle becomes narrower.

[34] Since no in situ ion composition measurements of Titan's ionosphere are available so far, we have investigated separately the effect of the cold ionospheric ion mass variation on the dispersion properties of the MTSI waves. As seen in Figure 4c, the frequency and growth rate of the fastest growing MTSI mode monotonically decrease with increasing ion mass approximately proportional to $M_I^{-1/3}$ in agreement with the analytical solution (3) of the dispersion relation (1). Also in agreement with the resonance condition (2), no significant ionospheric ion mass dependence of the dominant wave numbers was found in the case of the MTSI waves in the 1–28 amu range.

3.2. Ion-Ion Acoustic Instability

[35] Similar to the MTSI case, we analyze the model parameter dependence of the IIAI-type solution of the dispersion relation (1) using the hot electron limit. Figure 5 shows the ion beam velocity dependence of the real wave frequencies (Figure 5a) and wave numbers (Figure 5c) corresponding to the growth rates (Figure 5b) maximized over wave numbers of the ion acoustic plasma waves. The illustrated curves are represented as a function of wave propagation angle, α, relative to the beam/core drift velocity direction, i.e., $\alpha = \arccos(\mathbf{U}_b\mathbf{B}_0/U_bB_0)$, and each curve corresponds to a given beam velocity.

[36] It can be easily seen from Figure 5 that the ion acoustic waves can propagate in a wide range of propagation angles and the frequency and wave numbers only weakly depend on the wave propagation angles. This result can easily be understood if one uses the kinetic limit of the Z function, $Z(w) \cong i\sqrt{\pi} - 2w$ being valid for the case when the resonance term $w_{e,p,\mathrm{N}^+} = |\omega - kU_{e,b}|/\sqrt{2}\,V_{Te,p,\mathrm{N}^+}k \ll 1$,

written for hot, unmagnetized electrons, protons, and N^+ ions, when approximating the numerical solution of the dispersion relation (1). According to this approximation it can be shown that the wave number of the dominant mode is of the order of proton Debye length:

$$k_m \lambda_{Dp} = \sqrt{(1/2)}(1+\xi)^{1/2}. \tag{4}$$

The corresponding real wave frequency scales with the ionospheric ion plasma frequency:

$$\omega_m = \omega_{pI} \frac{k\lambda_{Dp}}{\left[1+\xi+\left(k\lambda_{Dp}\right)^2\right]^{1/2}}, \tag{5a}$$

where $\xi = (\boldsymbol{T}/($

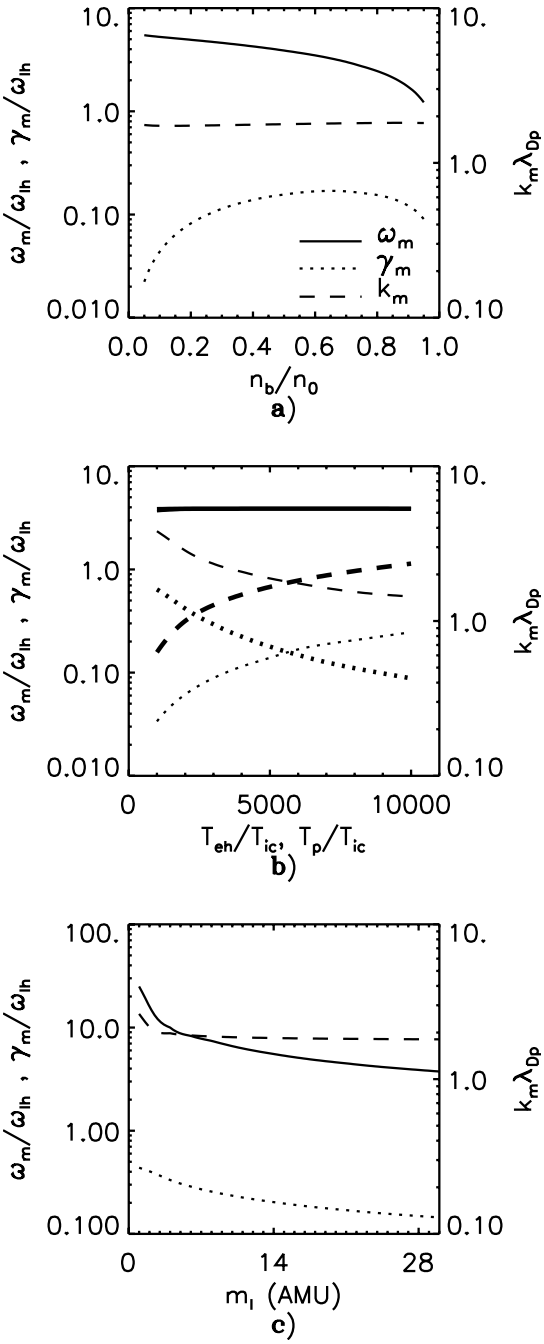

Figure 6. Dependence of the IIAI-type solution of the dispersion relation (1) on (a) beam density, n_b/n_e, (b) hot electron temperature, T_{eh}/T_I (thin lines), and beam proton temperature, T_p/T_I (thick lines), and (c) ionospheric ion mass, m_I/m_p. The wave frequency, $\omega_m/\omega_{\mathrm{LH}}$ (solid line), growth rate, $\gamma_m/\omega_{\mathrm{LH}}$ (dotted line), and wave number, $k_m\rho^*$ (dashed line), corresponding to the fastest growing mode are determined by maximizing the growth rate over the wave numbers and propagation angles relative to the beam drift velocity, α. Other plasma parameters are fixed and identical to the ones used in Figure 2.

resonance velocities decreases, and so does the growth rate. On the other hand, the wave frequency, ω_m, is almost insensitive to the electron and proton temperature variation. Regarding the physical behavior of k_m, we can conclude from Figure 6b that by increasing the hot electron temperature the wavelength of the dominant IIAI mode increased by a factor of $\sim$2.6. However, since the wave number of the dominant IIAI mode was normalized to the proton Debye length, a similar relative increase in the proton temperature increased the characteristic wavelength of the oscillations only by $\sim$8%.

[42] Finally, we also investigate the effect of the ionospheric ion mass variation on the IIAI wave properties (see Figure 6c). Here the main conclusion drawn is qualitatively similar to the one obtained in the MTSI case; namely, the frequency and growth rate of the ion acoustic waves monotonically decrease with the increasing ionospheric ion mass, while the dominant wave number is insensitive to the ion mass variation. The decrease in wave frequency is approximately proportional to $m_I^{-1/2}$ according to equation (5a). Some discrepancy between the analytically approximated and general solution occurs in the $m_I \sim 1-6$ amu range because the condition $kU_b \gg \omega$ used in the derivation of the approximated dispersion relation of the IIAI mode was no longer valid.

4. Summary and Discussion

[43] Cassini will be the first spacecraft to measure in situ plasma waves and charged particles within Titan's flowside interaction region (analogous to the dayside plasma mantles of Venus and Mars); therefore it is appropriate to anticipate these measurements using theoretical model calculations based on currently available experimental and theoretical knowledge. In this paper we have investigated possible mechanisms for generation of broadband plasma waves within the flowside mantle of Titan and carried out a parametric study of the possibly dominant beam-driven instability modes in a wide plasma parameter space within the framework of the linear Vlasov dispersion theory.

[44] Two different types of wave generation mechanisms were found to be existing within the flowside plasma mantle of Titan. One is the so-called modified two-stream instability (MTSI). In this case, among the different possible driver beam plasma components (protons, N^+ ions, and electrons) the dominant instability branch turned out to be the relative drift between the cold, magnetized electrons of ionospheric origin picked up rapidly by the streaming plasma and the cold ions originating from the upper atmosphere of Titan either born within the mantle by photoionization, electron impact ionization, and/or charge exchange or escaping into the hot magnetospheric/solar wind plasma from the ionosphere. Another instability type which may only become dominant in the absence of the cold electron population is generated by the hot, unmagnetized proton beam interacting with the background ionospheric ions via the mechanism of inverse Landau damping (beam resonant kinetic instability). This instability branch may be identified as an ion-ion acoustic instability (IIAI).

[45] Table 1 presents some physical plasma parameter ranges which were selected to mainly overlap the normalized plasma parameter space used in section 3 and presumably may be encountered by the Cassini spacecraft above the flowside ionosphere of Titan. On the basis of these model parameters we have solved the dispersion relation (1) and calculated the corresponding variations in the wave

Table 1. Plasma Parameter Ranges and Corresponding Wave Characteristics[a]

		MTSI Waves		IIAI Waves ($n_{ec} \approx 0$)	
	Parameter Range	Frequency, Hz	Wavelength, km	Frequency, Hz	Wavelength, km
External magnetic field	2–20 nT	0.2–3	1–12	12–13	1–2
Beam number density	0.06–0.6 cm^{-3}	0.6–0.9	3–4	5–18	1–2
Beam proton number density	0.03–0.3 cm^{-3}	~0.6	3–4	12–13	1–2
Beam proton temperature	35–350 eV	~0.6	3–4	12–13	1–2
Beam N^+ ion temperature	300–3000 eV	~0.6	3–4	12–13	1–2
Cold electron temperature	0.01–1 eV	0.4–0.8	1–13	· · ·	· · ·
Hot electron temperature	35–350 eV	· · ·	· · ·	11–13	0.5–1.5
Ionospheric ion temperature	0.01–1 eV	0.6–08	3–5	12–13	1–2
Ionospheric ion mass	1–28 AMU	0.6–3	3–4	12–82	~1
Beam ion drift velocity	30–420 km s^{-1}	0.4–1	3–5	11–14	1–2

[a]Plasma parameter ranges and corresponding wave characteristics are of the dominant modified two-stream instability (MTSI) and ion-ion acoustic instability (IIAI) modes. Parameter intervals were chosen to encompass the average plasma parameter values measured by Voyager 1 in the wake of Titan [see *Hartle et al.*, 1982] and predicted by ionospheric model calculations [see *Roboz and Nagy*, 1994].

characteristics (wave frequency and wavelength) of the fastest growing MTSI and IIAI modes, respectively. During the calculations the listed plasma parameters were changed one at a time while the rest of the parameters were kept at fixed values corresponding to the average plasma conditions observed by Voyager 1 spacecraft within the wake of Titan [*Hartle et al.*, 1982] and also were determined by the ionospheric model calculations [*Roboz and Nagy*, 1994]. (For a list of these average model values, see Figure 2 caption.) Since the ion acoustic–type waves are strongly damped by even a small amount of cold electrons (illustrated in Figure 2), the two modes cannot exist together. The MTSI mode may be dominant closer to the topside ionosphere, while the IIAI mode may be operational only at higher altitudes above the ionosphere, where the cold electron density $n_{ec} \approx 0$. It can be seen that within the parameter range of Table 1 the wave frequency of the dominant MTSI mode depends mostly on strength of the external magnetic field and the ionospheric ion mass, the frequency being approximately proportional to the lower hybrid frequency, $\nu_{LH} = (1/2\pi)(m_e/m_p)^{1/2}(eB_0/m_e c)$, and inversely proportional to the cubic root of the ionospheric ion mass according to equation (3). It can be similarly shown, using the resonance condition (2), that the dominant MTSI wavelength increases approximately proportional with the square root of the cold electron temperature and inversely proportional with the magnetic field. In the case of the IIAI mode the dominant wave frequency (with equation (5a) being proportional to the ionospheric ion plasma frequency, $\nu_{pI} = (1/2\pi)(4\pi n_I e^2/m_I)^{1/2}$, at fixed total plasma density (i.e., $n_p = n_b + n_I = \text{const}$)), decreases with increasing beam density (n_b) and ionospheric ion mass (m_I). The dominant wavelength of the IIAI mode is less sensitive to changes in the model parameters of Table 1 than in the case of the MTSI waves.

[46] In order to predict possible Cassini wave activity observations within the flowside plasma mantle region of Titan we have partly based our calculations on the results of the two-dimensional MHD model of *Cravens et al.* [1998] describing the large-scale interaction of the corotating magnetospheric plasma of Saturn with the ionosphere of Titan. According to this model a magnetic barrier is formed in the topside ionosphere/mantle region, with peak magnetic field values in the ram direction of ~18 nT occurring at altitudes around 1900 km. We took this altitude as the lower boundary of the interaction region, acknowledging, though, the fact that very likely, there is no sharp ionopause at Titan. The ion species included in the model are generic light (~1 amu mass, e.g., H^+), medium (~14 amu mass, e.g., N^+), and heavy (~28 amu mass, e.g., H_2CN^+) species. Figure 7a illustrates the altitude variation of the plasma composition, magnetic field, and bulk velocity used as fixed plasma background values when solving the general dispersion relation (1). Below 2900 km altitude we followed Cravens et al.'s model; above 2900 km, reasonably extrapolated plasma parameter values were taken for the sake of definiteness. The temperatures of the ions and electrons were taken to be altitude-independent, with values taken identical to those presented in Figure 2. The altitude profile of the plasma flow velocity was chosen to reflect the case corresponding to zenith angles between the ram flow and flank direction (see the dashed rectangle in Figure 1 for a schematic illustration). We also arbitrarily chose 2900 km as the boundary altitude where the density of the cold ionospheric electrons becomes zero and hot, magnetospheric electrons provide the charge neutralization. At higher altitudes, cold electrons may be absent because of their strong magnetization (their gyroradius being of the order of a tenth of 1 km). However, cold ions originating from Titan may escape more deeply into the hot streaming plasma because of their much larger gyroradius (about a few to a few tens of kilometers). We expect that by analogy to the case of the dayside plasma mantles of Venus and Mars the depth of penetration of the heavy ionospheric ions into the magnetosphere of Saturn or solar wind is further enhanced by the turbulent diffusion through the magnetic field lines, reaching distances of the order of a few hundred kilometers.

[47] Our prediction is that the most pregnant feature of the altitude variation of the locally dominant instability types (shown in Figure 7b) is the abrupt separation of the plasma mantle into regions dominated by either the MTSI or IIAI mode, caused by the presence/absence of the cold ionospheric electron population. Closer to the topside ionosphere (where cold electrons are present), the MTSI is dominant. The typical frequency slowly decreases from 2 Hz to below 1 Hz, while the wavelength increases from ~0.5 to ~2.5 km with altitudes increasing from 1900 to 2900 km. In the absence of cold electrons the dominant ion acoustic–type wave frequencies decrease from about 12 to 5 Hz,

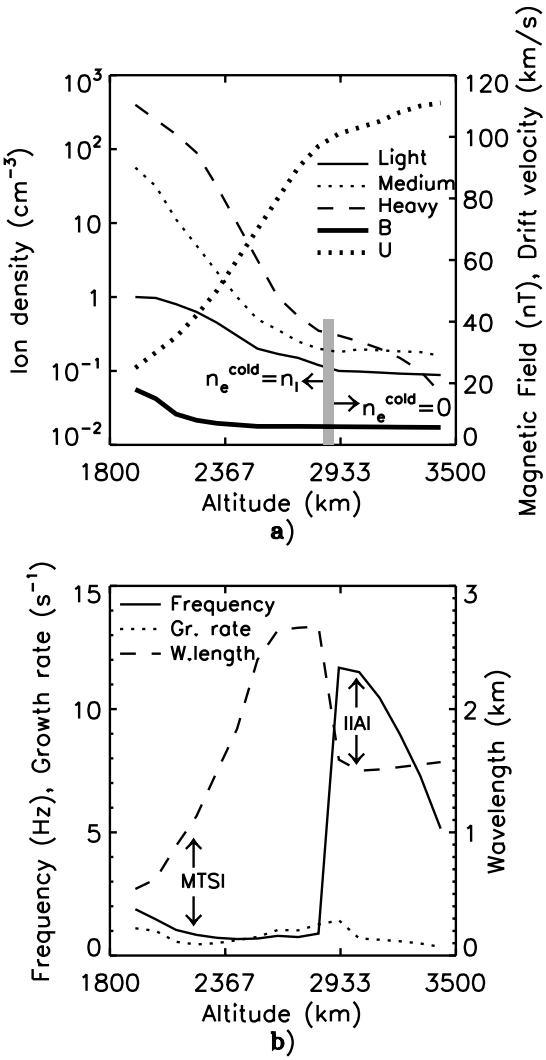

Figure 7. (a) Theoretical plasma composition, magnetic field, and beam drift velocity within the flowside interaction region of Titan (spatial location schematically illustrated by the dashed rectangle in Figure 1). Below 2900 km, plasma parameter values were taken from *Cravens et al.* [1998]; above 2900 km, extrapolation was used. (b) Altitude dependence of wave frequency, growth rate, and wavelength of the fastest-growing modes of the MTSI and IIAI within the flowside plasma mantle of Titan corresponding to the model plasma parameters presented in Figure 7a. The boundary altitude where the density of the cold ionospheric electrons becomes zero was arbitrarily chosen at 2900 km.

while the wavelength remains practically unchanged at a value of ~1.5 km when the altitudes increased from 2900 to 3400 km.

[48] We can also predict significant difference in the wave propagation behavior of the two instability modes. The direction of propagation of the dominant MTSI waves is determined by the external magnetic field and the beam velocity. The phase velocity vector ($\mathbf{v}_{ph}^{MTSI}$) of the fastest growing mode aligns with the drift velocity vector ($\mathbf{U}_b$). Using analytic approximations (2) and (3), one can easily show that $v_{ph}^{MTSI} \sim (1/2)^{4/3}(n_I/n_e)^{1/3}(n_b/n_e)(m_p/m_I)^{1/3}\kappa^{-2/3}$ $U_b \ll U_b$. Moreover, for a given direction of the magnetic field the angle corresponding to the propagation of the fastest growing mode can be approximated as $\cos\theta_{max} = (k_{||}/k)_{max} \sim (1/4\sqrt{2})(n_b/n_e)(U_b/V_{Te})$ on the basis of the condition of Landau resonance of the magnetized electrons corresponding to the maximum growth rate of the MTSI discussed in section 3.1. Since the direction of wave propagation of the most unstable lower hybrid wave modes relative to the magnetic field lines decreases with the increasing drift velocity of the beam, it can be expected that the MTSI waves may propagate less perpendicularly and in a wider angle range relative to the external magnetic field when the driver beam velocity is larger, for example, when Titan is located within the solar wind. On the other hand, wave propagation and polarization directions closer to the plane perpendicular to the external magnetic field are to be expected at lower beam velocities, corresponding to the case when Titan is within the magnetosphere of Saturn.

[49] It is also important to determine the characteristic wave energy propagation direction of the dominant MTSI mode. This can be easily estimated from the ratio of the parallel to transverse component of wave group velocity relative to the magnetic field lines. Again, using the analytically approximated solutions (2) and (3) of the general dispersion relation (1) for the dominant MTSI modes in the electrostatic limit, $(\omega_{pe}/kc)^2 \ll 1$, we can obtain $(v_{g||}/v_{g\perp})_{MTSI} \sim -(2/5)(k^2/k_{||}k_\perp)[1-(5/2)(k_{||}/k)^2]$, $k)^2]$, where $v_{g||} \equiv (\partial\omega/\partial k_{||})_{k\perp=const}$, $v_{g\perp} \equiv (\partial\omega/\partial k_\perp)_{k||=const} \sim (5/3)(k_\perp/k)v_{ph}^{MTSI}$, and $k = (k_{||}^2 + k_\perp^2)^{1/2}$. It can be easily seen that with decreasing wave propagation angles of the dominant mode, θ_{max} (and correspondingly with increasing $(k_{||}/k)_{max}$, caused, for example, by an increasing beam velocity), the parallel component of the group velocity monotonically decreases compared to the perpendicular component. More specifically, i.e., in the case when Titan is within Saturn's magnetosphere, lower beam velocities may occur; for example, when $u = 0.5$, the parallel to perpendicular group velocity ratio is $v_{g||}/v_{g\perp} \sim 6$. This means that the wave energy is convected mostly aligned with the magnetic field draping the topside ionosphere. In the case of higher beam velocities most probably occurring when Titan enters into the solar wind, for example, when $u = 3$, the wave energy propagates predominantly perpendicular to the draping magnetic field, $v_{g||}/v_{g\perp} \sim 0.6$, and can be more effectively absorbed by the tail part of the ionospheric electron population being in Landau resonance with the waves. The possibility of the topside heating of the ionospheres of Venus and Mars by absorbed lower-hybrid-type plasma waves was discussed by *Szegő et al.* [1991] and *Shapiro et al.* [1995] in order to explain the discrepancy between the higher measured ionospheric electron temperatures and electron temperatures calculated by thermal models using UV heating as the only dominant heat source of the ionosphere. An estimation of the magnitude of heat inflow from the streaming plasma into the topside ionosphere of Titan mediated by fluid-type MTSI waves generated above the ionosphere will be given in a forthcoming paper.

[50] In the case of the IIAI waves, since all plasma components can be considered as unmagnetized, the only

reference direction we have is the drift velocity of the streaming plasma. According to Figure 5b the IIAI waves can propagate in a wide range of directions. However, while at lower drift velocities (order of $u = 0.5$ and 1) the fastest growing mode propagates parallel with the streaming plasma, at higher drift velocities (order of $u = 2$ and 3) the propagation direction of the dominant IIAI instability mode becomes more oblique to the drift velocity vector. In contrast to the MTSI waves the phase and the group velocities of the ion acoustic oscillations are aligned and relate to each other approximately as $v_g^{\mathrm{IIAI}} \equiv (\partial\omega/\partial k) \sim (1 + \xi)(1 + \xi + k^2\lambda_{Dp}^2)^{-1} v_{ph}^{\mathrm{IIAI}} \sim (2/3) v_{ph}^{\mathrm{IIAI}}$, where the phase velocity is $v_{ph}^{\mathrm{IIAI}} = \omega_{pI}\, \lambda_{Dp}/(1 + \xi + k^2\lambda_{Dp}^2)^{1/2}$, according to the approximated analytical forms (4) and (5) of the IIAI-type solution of dispersion relation (1).

[51] Finally, it is important to emphasize that the linear Vlasov model of the possible wave generation mechanisms operating within the flowside plasma mantle of Titan has strong limitations. On one hand, the nonlinear turbulent processes can significantly alter (shift and broaden) the wave spectra calculated by the linear theory, so one can only consider these predictions as best estimates. On the other hand, the linear model is not self-consistent in the sense that it cannot give an account for the feedback of the waves on the physical properties of plasma background. In a forthcoming paper we will show that these wave modes can significantly alter the local bulk properties of the different plasma components such as drift velocity and random energy content due to collective and stochastic energy transfer through wave-particle interaction from the streaming plasma of either magnetospheric or solar wind origin to the cold ionospheric plasma. Using hybrid particle-in-cell simulation, we will study the linear and nonlinear time evolution of the instability modes generated within the flowside plasma mantle of Titan. Estimations for the saturated wave electric field spectral energy density level will be given. Also, the energy range where significant superthermal particles are to be expected because of acceleration by wave electric fields will be determined.

[52] **Acknowledgments.** The authors gratefully acknowledge the support provided by OTKA grant 32634.

[53] Arthur Richmond thanks Thomas Cravens and Joseph Huba for their assistance in evaluating this paper.

References

Acuna, M. H., and N. F. Ness (1980), The magnetic field of Saturn: Pioneer 11 observations, *Science*, *207*, 444–446.

Bingham, R., V. D. Shapiro, V. N. Tsytovich, U. de Angelis, M. Gilman, and V. I. Shevchenko (1991), Theory of wave activity occurring in the AMPTE artificial comet, *Phys. Fluids B*, *3*(7), 1728–1738.

Brecht, S. H., J. G. Luhmann, and D. J. Larson (2000), Simulation of the Saturnine magnetospheric interaction with Titan, *J. Geophys. Res.*, *105*, 13,119–13,130.

Cravens, T. E., C. J. Lindgren, and S. A. Lendvina (1998), A two-dimensional multi-fluid MHD model of Titan's plasma environment, *Planet. Space Sci.*, *46*, 1193–1206.

Dóbé, Z., K. B. Quest, V. D. Shapiro, K. Szegő, and J. D. Huba (1999), Interaction of the solar wind with unmagnetized planets, *Phys. Rev. Lett.*, *83*, 260–263.

Gary, S. P., and N. Omidi (1987), The ion/ion acoustic instability, *J. Plasma Phys.*, *37*, 45–61.

Hartle, R. E., E. C. Sittler Jr., K. W. Ogilvie, and J. D. Scudder (1982), Titan's ion exosphere observed from Voyager 1, *J. Geophys. Res.*, *87*, 1383–1394.

Huba, J. D. (1993), Generation of waves in the Venus mantle by ion acoustic beam instability, *Geophys. Res. Lett.*, *20*, 1751–1754.

Hunten, D. M., M. G. Tomasko, F. M. Flasar, R. F. Samuelson, and D. E. Strobel (1984), Titan, in *Saturn*, edited by T. Gehrels and M. S. Matthews, pp. 671–759, Univ. of Ariz. Press, Tucson.

Kabin, K. P., P. L. Israelevich, A. I. Ershkovich, F. M. Neubauer, T. I. Gombosi, D. L. de Zeeuw, and K. G. Powel (2000), Titan's magnetic wake: Atmospheric or magnetospheric interaction, *J. Geophys. Res.*, *105*, 10,761–10,770.

Keller, C. N., T. E. Cravens, and L. Gan (1992), A model of the ionosphere of Titan, *J. Geophys. Res.*, *97*, 12,117–12,135.

Kopp, A., and W.-H. Ip (2001), Asymmetric mass loading effect at Titan's ionosphere, *J. Geophys. Res.*, *106*, 8323–8332.

Ledvina, S. A., and T. E. Cravens (1998), A three-dimensional MHD model of plasma flow around Titan, *Planet. Space Sci.*, *46*, 1175–1192.

Lundin, R., A. Zakharov, R. Pellinen, S. W. Barabash, H. Borg, E. M. Dubinin, B. Hultquist, H. Koskinen, I. Liede, and N. Pissarenko (1990), ASPERA/Phobos measurements of the ion outflow from the Martian ionosphere, *Geophys. Res. Lett.*, *17*, 873–876.

McBride, J. B., and E. Ott (1972), Electromagnetic and finite β_e effects on the modified two stream instability, *Phys. Lett. A*, *39*, 363–364.

Nagy, A. F., and T. E. Cravens (1998), Titan's ionosphere: A review, *Planet. Space Sci.*, *46*, 1149–1155.

Nagy, A. F., T. I. Gombosi, K. Szegő, R. Z. Sagdeev, V. D. Shapiro, and V. I. Shevchenko (1990), Venus mantle–Mars planetosphere: What are the similarities and differences?, *Geophys. Res. Lett.*, *17*, 865–868.

Ness, N. F., M. H. Acuna, K. W. Behannon, and F. M. Neubauer (1982), The induced magnetosphere of Titan, *J. Geophys. Res.*, *87*, 1369–1381.

Neubauer, F. M. (1992), Titan's magnetospheric interaction, *Eur. Space Agency Spec. Publ., ESA SP-338*, 267–272.

Neubauer, F. M., D. A. Gurnett, J. D. Scudder, and R. E. Hartle (1984), Titan's magnetospheric interaction, in *Saturn*, edited by T. Gehrels and M. S. Matthews, pp. 760–787, Univ. of Ariz. Press, Tucson.

Quest, K. B., V. D. Shapiro, K. Szegő, and Z. Dóbé (1997), Microphysics of the Venusian and Martian mantles, *Geophys. Res. Lett.*, *24*, 301–304.

Roboz, A., and A. F. Nagy (1994), The energetics of Titan's ionosphere, *J. Geophys. Res.*, *99*, 2087–2094.

Sagdeev, R. Z., V. D. Shapiro, V. I. Shevchenko, A. Zacharov, P. Király, K. Szegő, A. F. Nagy, and R. Grard (1990), Wave activity in the neighborhood of the bowshock of Mars, *Geophys. Res. Lett.*, *17*, 893–896.

Shapiro, V. D., K. Szegő, S. K. Ride, A. F. Nagy, and V. I. Shevchenko (1995), On the interaction between the shocked solar wind and the planetary ions in the dayside of Venus, *J. Geophys. Res.*, *100*, 21,289–21,298.

Sittler, E. C., R. E. Hartle, A. F. Viñas, R. E. Johnson, H. T. Smith, and I. Mueller-Wodard (2004), Titan interaction with Saturn's magnetosphere: Mass loading and ionopause location, paper presented at Titan Meeting at ESTEC, Eur. Space Res. and Technol. Cent., Noordwijk, Holland, 13–17 April.

Spenner, K., W. C. Knudsen, K. L. Miller, V. Novak, C. T. Russel, and R. C. Elphic (1980), Observation of the Venus mantle, boundary region between solar wind and ionosphere, *J. Geophys. Res.*, *85*, 7655–7662.

Szegő, K., V. D. Shapiro, V. I. Shevchenko, R. Z. Sagdeev, W. T. Kasprzak, and A. F. Nagy (1991), Physical processes in the plasma mantle of Venus, *Geophys. Res. Lett.*, *18*, 2305–2308.

Szegő, K., Z. Dóbé, J. Huba, K. Quest, and V. D. Shapiro (2000), Wave activity in the dayside mantle of Venus, Mars, and Titan, *Adv. Space Res.*, *26*, 1609–1612.

Wolf, D. A., and F. M. Neubauer (1982), Titan's highly variable plasma environment, *J. Geophys. Res.*, *87*, 881–885.

Wu, C. S., Y. M. Zhou, S. T. Tsai, S. G. Guo, D. Winske, and K. Papadopoulos (1983), A kinetic cross-field streaming instability, *Phys. Fluids*, *26*, 1259–1267.

Zhang, M. H. G., J. G. Luhmann, A. F. Nagy, J. R. Spreiter, and S. S. Stahara (1993), Oxygen ionization rates at Mars and Venus: Relative contributions of impact ionization and charge exchange, *J. Geophys. Res.*, *98*, 3311–3318.

Z. Dóbé, GE Hungary Co., Automative Technology, Váci út 77, H-1340 Budapest, Hungary. (zoltan.dobe@lighting.ge.com)

K. Szegő, MTA KFKI Research Institute for Particle and Nuclear Physics, POB 49, H-1525 Budapest, Hungary. (szego@rmki.kfki.hu)